JCI The Journal of Clinical Investigation

The Schlemm's canal is a VEGF-C/VEGFR-3–responsive lymphatic-like vessel

Aleksanteri Aspelund, Tuomas Tammela, Salli Antila, Harri Nurmi, Veli-Matti Leppänen, Georgia Zarkada, Lukas Stanczuk, Mathias Francois, Taija Mäkinen, Pipsa Saharinen, Ilkka Immonen, Kari Alitalo

J Clin Invest. 2014;124(9):3975-3986. https://doi.org/10.1172/JCI75395.

Research Article

In glaucoma, aqueous outflow into the Schlemm's canal (SC) is obstructed. Despite striking structural and functional similarities with the lymphatic vascular system, it is unknown whether the SC is a blood or lymphatic vessel. Here, we demonstrated the expression of lymphatic endothelial cell markers by the SC in murine and zebrafish models as well as in human eye tissue. The initial stages of SC development involved induction of the transcription factor PROX1 and the lymphangiogenic receptor tyrosine kinase VEGFR-3 in venous endothelial cells in postnatal mice. Using gene deletion and function-blocking antibodies in mice, we determined that the lymphangiogenic growth factor VEGF-C and its receptor, VEGFR-3, are essential for SC development. Delivery of VEGF-C into the adult eye resulted in sprouting, proliferation, and growth of SC endothelial cells, whereas VEGF-A obliterated the aqueous outflow system. Furthermore, a single injection of recombinant VEGF-C induced SC growth and was associated with trend toward a sustained decrease in intraocular pressure in adult mice. These results reveal the evolutionary conservation of the lymphatic-like phenotype of the SC, implicate VEGF-C and VEGFR-3 as critical regulators of SC lymphangiogenesis, and provide a basis for further studies on therapeutic manipulation of the SC with VEGF-C in glaucoma treatment.

The Schlemm's canal is a VEGF-C/VEGFR-3–responsive lymphatic-like vessel

Aleksanteri Aspelund,[1] Tuomas Tammela,[1] Salli Antila,[1] Harri Nurmi,[1] Veli-Matti Leppänen,[1] Georgia Zarkada,[1] Lukas Stanczuk,[2] Mathias Francois,[3] Taija Mäkinen,[2] Pipsa Saharinen,[1] Ilkka Immonen,[4] and Kari Alitalo[1]

[1]Wihuri Research Institute and Translational Cancer Biology Program, Biomedicum Helsinki, University of Helsinki, Helsinki, Finland. [2]Department of Immunology, Genetics and Pathology, University of Uppsala, Uppsala, Sweden. [3]Genomics of Development and Disease Division, University of Queensland, Brisbane, Australia. [4]Department of Ophthalmology, Helsinki University Central Hospital, Helsinki, Finland.

In glaucoma, aqueous outflow into the Schlemm's canal (SC) is obstructed. Despite striking structural and functional similarities with the lymphatic vascular system, it is unknown whether the SC is a blood or lymphatic vessel. Here, we demonstrated the expression of lymphatic endothelial cell markers by the SC in murine and zebrafish models as well as in human eye tissue. The initial stages of SC development involved induction of the transcription factor PROX1 and the lymphangiogenic receptor tyrosine kinase VEGFR-3 in venous endothelial cells in postnatal mice. Using gene deletion and function-blocking antibodies in mice, we determined that the lymphangiogenic growth factor VEGF-C and its receptor, VEGFR-3, are essential for SC development. Delivery of VEGF-C into the adult eye resulted in sprouting, proliferation, and growth of SC endothelial cells, whereas VEGF-A obliterated the aqueous outflow system. Furthermore, a single injection of recombinant VEGF-C induced SC growth and was associated with trend toward a sustained decrease in intraocular pressure in adult mice. These results reveal the evolutionary conservation of the lymphatic-like phenotype of the SC, implicate VEGF-C and VEGFR-3 as critical regulators of SC lymphangiogenesis, and provide a basis for further studies on therapeutic manipulation of the SC with VEGF-C in glaucoma treatment.

Introduction

Glaucoma is a group of heterogeneous diseases characterized by chronic, degenerative optic neuropathy with resultant loss of visual field (1). It is the second leading cause of blindness in the world (2), affecting approximately 2.6% of the population over 40 years of age worldwide (3). The most important, and the only modifiable, causal risk factor for glaucoma is elevated intraocular pressure (IOP) (1).

IOP is determined by the balance between the rate of production and rate of removal of the aqueous humor (AH). AH is prod¡¡uced by the ciliary epithelium, sieved through the trabecular meshwork (TM), taken up by the Schlemm's canal (SC), and drained into episcleral (ES) veins via aqueous veins (AVs) (1, 4). The trabecular outflow pathway accounts for 70%–90% of AH removal in humans. In glaucoma, aqueous outflow resistance increases, resulting in increased IOP and subsequent optic neuropathy (5). Therefore, current glaucoma treatments are aimed at lowering IOP. Medical and surgical treatments for open-angle glaucoma reduce the short- or medium-term risk for optic nerve damage (6). However, normalization of IOP and arrest of glaucoma development is often not achieved. Moreover, current medical glaucoma treatment strategies are hindered by patient noncompliance with daily administration of eye drops (7).

The SC is a unique ring-shaped, endothelium-lined vessel that encircles the cornea (8). It is the final barrier for the AH before returning to systemic circulation, but its specific contribution to AH outflow resistance is unknown (4). Interestingly, glaucoma patients have a smaller SC (9), and agenesis or hypoplasia of the SC has been implicated in primary congenital glaucomas (10–13). However, it is still unknown whether the SC is a component of the blood or the lymphatic vascular system (1, 4, 14).

The SC shares striking structural and functional similarities with lymphatic vessels: it forms a blind-ended tube that does not contain blood, but transports AH and antigen-presenting cells into venous circulation (1, 15, 16). Furthermore, the SC has a continuous endothelial cell (EC) monolayer that lacks fenestrations, lies on a discontinuous basement membrane, is not enclosed by pericytes or smooth muscle cells, and is subjected to a basal-to-apical direction of flow, like lymphatic capillaries (1, 4, 17, 18). Moreover, connecting fibrils extending from SC ECs into the surrounding cribriform plexus may be involved in preventing SC collapse (17), analogously to the anchoring filaments found in lymphatic vessels (4, 19, 20).

Recent years have seen substantial progress in understanding the molecular regulation of lymphangiogenesis (21). The genetic programs that determine lymphatic EC (LEC) differentiation and growth, making them distinct from blood vessels, involve a number of newly described signal transduction pathways (22). LECs differentiate from blood vascular ECs (BECs) in the cardinal vein during E9.5–E10.5, when distinct subpopulations of ECs in the anterior cardinal veins commit to the lymphatic lineage and sprout

▶ Related Commentary: p. 3701

Authorship note: Tuomas Tammela and Salli Antila contributed equally to this work.
Conflict of interest: Aleksanteri Aspelund, Tuomas Tammela, Ilkka Immonen, and Kari Alitalo have filed a patent application for the therapeutic use of VEGF-C in ocular hypertension and glaucoma. Kari Alitalo is a consultant of Herantis Pharma Ltd.
Submitted: January 27, 2014; **Accepted:** May 30, 2014.
Reference information: *J Clin Invest*. 2014;124(9):3975–3986. doi:10.1172/JCI75395.

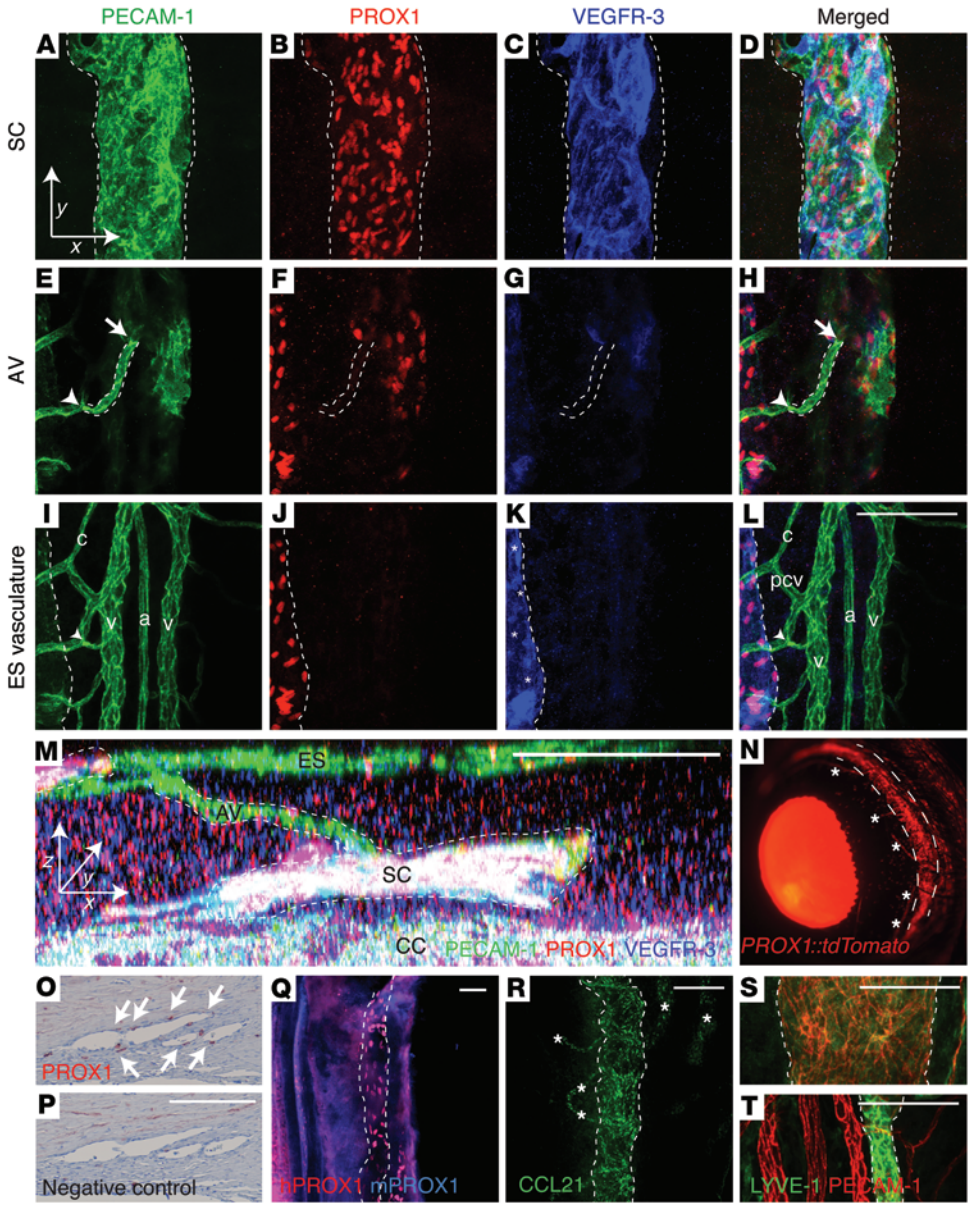

Figure 1. SC ECs display molecular features of lymphatic endothelium. (**A**–**M**) Whole-mount immunofluorescence staining of the adult murine eye using antibodies against PECAM-1, PROX1, and VEGFR-3. The entire thickness of the limbus was visualized by confocal imaging into 1 *z* stack. Subsets with the SC (**A**–**D**), the AV (**E**–**H**), and the ES vasculature (**I**–**L**) are shown. The joining point of the AV into the SC (arrow) and the joining point of the AV into the ES vein (arrowhead) are indicated. Dashed outlines denote the SC and ES lymphatic vessels. c, capillary; pcv, postcapillary venule; v, vein; a, artery. (**M**) AH drainage route in a 90° *y*-axis projection of the confocal stack in **A**–**L**. *xyz* axes are shown for orientation between **A**–**L** and **M**. (**N**) The SC (dashed outline) and ES lymphatic vessels (asterisks) in vivo in *Prox1-CreER^{T2} LSL-tdTomato* lineage tracer mice after 4-OHT administration. (**O** and **P**) Immunohistochemical PROX1 staining and negative control staining of the SC in a human eye. Arrows indicate PROX1 expression in SC ECs. (**Q**) Visualization of zebrafish SC by staining with antibodies against human and mouse PROX1. (**R**–**T**) Immunofluorescence staining of murine SC and ES lymphatic vessels using antibodies against CCL21 (**R**) and LYVE-1 (**S** and **T**). Scale bars: 100 μm (**A**–**L**, **S**, and **T**); 50 μm (**M**); 200 μm (**N**–**R**).

to form primordial lymphatic structures (23, 24). Their development from large embryonic veins involves induction of the prospero-related homeobox 1 transcription factor (PROX1) (25). Subsequent sprouting is driven by the lymphangiogenic growth factor VEGF-C, which stimulates VEGFR-3 tyrosine kinase signaling in LECs (21, 23, 24, 26). Importantly, through the discovery of lymphangiogenic factors, it has become possible to treat lymphedema with lymphatic growth factors (20, 27–29). Based on these recent advances, we sought to investigate the therapeutic implications of the possibility of the SC being a lymphatic vessel.

Results

SC ECs display molecular features of lymphatic endothelium. To investigate whether the SC is a lymphatic vessel, we analyzed the expression of LEC markers in mouse, zebrafish, and human eyes. The SC in mouse eyes was visualized using whole-mount immunofluorescence staining of the anterior segment of the eye. By laser-scanning confocal microscopy (LSCM), the SC was found to express platelet-endothelial cell adhesion molecule–1 (PECAM-1), the lymphatic master transcription factor PROX1, and the lymphangiogenic receptor tyrosine kinase VEGFR-3 (Figure 1, A–D). At regular intervals, the SC was observed to connect with AVs of blood capillary caliber (≈9 μm wide), expressing PECAM-1, very low PROX1, and no VEGFR-3 (Figure 1, E–H). The AVs were observed to drain into larger ES postcapillary venules (≈11 μm wide) on the surface of the eye (Figure 1, I–L). The ES lymphatic vessels were positive and ES blood vessels negative for PROX1 and VEGFR-3 (Figure 1, I–L), providing internal controls for the stainings. Overall, the SC and the AVs were detected between choriocapillaries (CCs) and the ES vasculature (Figure 1M), where the SC forms a uniform duct that runs at the base of the iris throughout the limbal circumference. Furthermore, we used *Prox1-CreER^{T2} LSL-tdTomato* (30, 31) Cre reporter mice to visualize the SC in vivo and to validate that the *Prox1-CreER^{T2}* allele could be used to

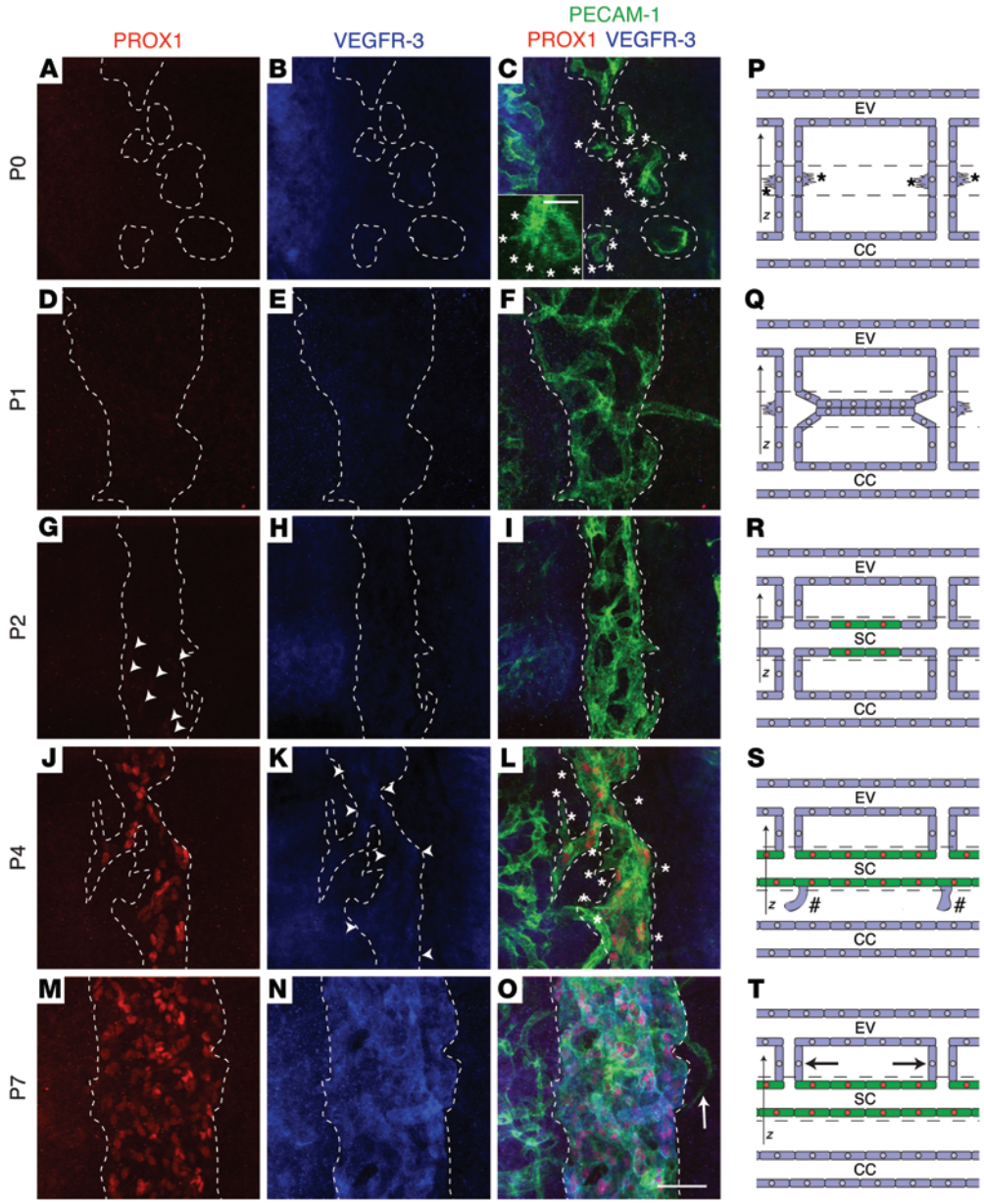

Figure 2. The SC develops postnatally from transscleral veins. (**A**–**O**) Immunofluorescence staining with antibodies against PECAM-1 (green), PROX1 (red), and VEGFR-3 (blue) were used to visualize SC development. (**P**–**T**) SC developmental stages. Dashed lines denote the subset of confocal *z* stacks selected for SC visualization. Blue cells, PROX1$^-$ BECs; green cells, PROX1$^+$ LEC-like cells. EV, ES vein. For 3D volume renderings of entire confocal *z* stacks with CCs and ES veins, see Supplemental Videos 1–5. (**A**–**C** and **P**) At P0, lateral sprouting (asterisks and inset in **C**) of transcleral veins toward adjacent transcleral veins was observed. (**D**–**F** and **Q**) At P1, connection of adjacent transcleral veins by strings of future SC ECs was apparent. (**G**–**I** and **R**) At P2, maturation and induction of PROX1 expression (arrowheads) was observed. (**J**–**L** and **S**) P4 revealed lumenization and expression of PROX1, induction of VEGFR-3 (arrowheads), regression of connections to CCs (hashtags), and lateral sprouting (asterisks). (**M**–**O** and **Y**) Mature SC at P7. Note that the AVs (arrow) did not regress. Scale bars: 50 μm (**A**–**O**), 12.5 μm (**C**, inset).

achieve lymphatic-specific, tamoxifen-inducible conditional gene deletion also in SC ECs. In these mice, SC and ES lymphatic vessels were specifically and effectively labeled (Figure 1N).

PROX1 expression was also detected in human SC ECs (Figure 1, O and P). Furthermore, the zebrafish SC analog could be visualized using whole-mount immunofluorescence staining with 2 independent PROX1 antibodies (Figure 1Q), which indicates that the lymphatic identity of the SC is conserved in vertebrate evolution.

Further immunofluorescence analysis revealed strong and specific staining for the secreted chemokine ligand CCL21, but little or no expression of the lymphatic hyaluronan receptor LYVE-1, and no expression of the transmembrane O-glycoprotein podoplanin (PDPN) by SC ECs, which expressed abundant levels of the cell matrix adhesion receptor integrin α9, but mostly low levels of the forkhead box transcription factor FOXC2 (Figure 1, R–T, and Supplemental Figure 1, A–C; supplemental material available online with this article; doi:10.1172/JCI75395DS1). We also injected 4-hydroxytamoxifen (4-OHT) into *Sox18-CreER^{T2} LSL-tdTomato* (32) lineage tracing mice at P2–P4, around the time when PROX1 is induced. Analysis at P7 indicated that the *Sox18* transcription factor promoter was active at the time of venous EC commitment to the SC lineage (Supplemental Figure 1D). Similar to lymphatic capillaries, SC ECs were not covered by NG2-positive pericytes or SMA-positive vascular smooth muscle cells (Supplemental Figure 2, A and B). SC ECs displayed zipper-type EC cell-cell junctions and were ensheathed by a thin layer of collagen IV (Supplemental Figure 2, C and D), like collecting lymphatic vessels. Whereas VEGFR-2 was expressed in nearly all blood and lymphatic vessels around the limbus, VEGFR-3 expression was restricted to SC ECs and ES lymphatic vessels (Supplemental Figure 3B).

The SC develops postnatally from transscleral veins. The characterization of SC developmental morphogenesis has previously been limited to serial sections (18), which provide insufficient information. The development of the lymph sacs has recently been

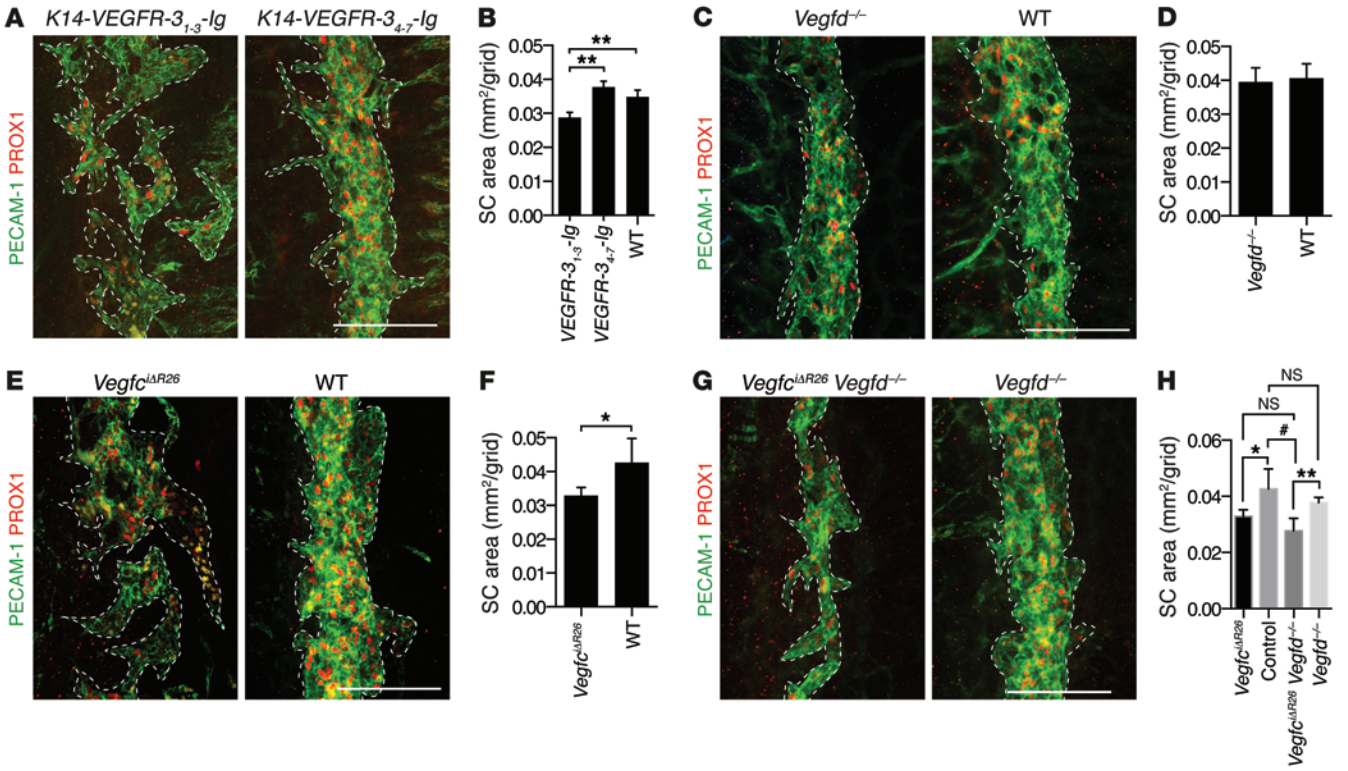

Figure 3. The lymphangiogenic growth factor VEGF-C is critical for SC development. (**A** and **B**) SC morphology (**A**) and mean area (**B**; data from 1 litter) in transgenic *K14-VEGFR-3$_{1-3}$-Ig* mice (n = 3), their WT littermate controls (n = 3), and *K14-VEGFR-3$_{4-7}$-Ig* mice (n = 4) at P7. (**C** and **D**) SC morphology (**C**) and mean area (**D**; data from 2 litters) in *Vegfc$^{i\Delta R26}$* (n = 4) and control *Vegfc$^{fl/fl}$* littermate (n = 5) mice at P7, after induction of Cre activity from P1 to P5 with daily 4-OHT injections. (**E** and **F**) SC morphology (**E**) and mean area (**F**; data from 1 litter) in *Vegfd$^{-/-}$* (n = 6) and littermate WT (n = 3) mice. (**G** and **H**) SC morphology (**G**) and mean area (**H**; data from 3 litters, and data from **F** included for comparison) in *Vegfc$^{i\Delta R26}$ Vegfd$^{-/-}$* (n = 8) and control littermate *Vegfc$^{fl/fl}$ Vegfd$^{-/-}$* (n = 5) mice at P7 after induction of Cre activity. Scale bars: 100 μm (**A**, **C**, **E**, and **G**). $^*P < 0.05$; $^{**}P < 0.01$; $^{\#}P < 0.0001$.

refined by selective plane illumination–based ultramicroscopy (23). We next set out to visualize the development of the SC in mice by applying LSCM to whole-mount immunofluorescence stained samples, which allowed us to generate 3D volume renderings of the confocal stacks. Formation of the SC was traced back to P0, when a circular network of sprouts extended from the limbal CC toward ES veins to connect them (Figure 2, A–C and P, Supplemental Video 1, and Supplemental Figure 4, A–D). At P1, these transscleral vessels had begun to sprout laterally toward each other to form EC strings at the site of the future SC (Figure 2, D–F and Q, Supplemental Video 2, and Supplemental Figure 4, E–H). By P2, the sprouting ECs had coalesced to form a rudimentary SC, and connections to the CCs were lost. The transscleral vessels that remained attached to the rudimentary SC represented the future AVs (Figure 2, G–I and R, Supplemental Video 3, and Supplemental Figure 4, I–L). At P4, cells of the rudimentary SC furthest away from the 2 long posterior ciliary arteries were observed to express low levels of PROX1 (Figure 2J). The cells expressed PROX1 throughout the canal, weak VEGFR-3 expression was detected, and the canal had undergone further luminalization, as fragments of it were detected in the H&E-stained sections (Figure 2, J–L and S, Supplemental Video 4, and Supplemental Figure 4, M–P). By P7, the SC had grown in width and expressed high levels of VEGFR-3, resembling the mature SC and appearing as a uniform canal in H&E-stained sections (Figure 2, M–O and T, Supplemental Video 5, and Supplemental Figure 4, Q–T). PROX1 and VEGFR-3 expression levels were maintained in adult mice (Figure 1, B and C). VEGFR-2 was detected in the thick sections at all stages of SC development, in the CC, and in the ES vasculature (Supplemental Figure 4).

To further validate the blood vascular origin of SC ECs, we used *Prox1-CreER^{T2} Rosa26^{mTmG}* mice to perform lineage tracing. When 4-OHT was injected at P0, prior to the PROX1 induction in SC ECs at around P2, nearly complete GFP labeling of ES LECs was observed, but no GFP$^+$ SC ECs. However, additional injection of 4-OHT at P4, after PROX1 was induced, resulted in the labeling of both ES LECs and SC ECs (Supplemental Figure 5). These data indicate that SC ECs do not originate from preexisting lymphatic vasculature.

The lymphangiogenic growth factor VEGF-C is critical for SC development. The close resemblance between SC and lymph sac development (23) led us to hypothesize that the lymphangiogenic growth factor VEGF-C plays a critical role in SC development as well. *Vegfc$^{-/-}$* mouse embryos are characterized by failure to form the initial LEC sprouts (23, 24). However, these mice cannot be studied postnatally due to embryonic lethality. We therefore analyzed *Vegfc* heterozygous mice (referred to herein as *Vegfc$^{+/LacZ}$*; ref. 24), conditionally *Vegfc*-deleted mice (*Vegfc$^{i\Delta R26}$*; Supplemental Figure 6 and ref. 33), *Vegfd*-knockout mice (*Vegfd$^{-/-}$*; ref. 34), *Vegfc$^{i\Delta R26}$ Vegfd$^{-/-}$* double-knockout mice, transgenic mice

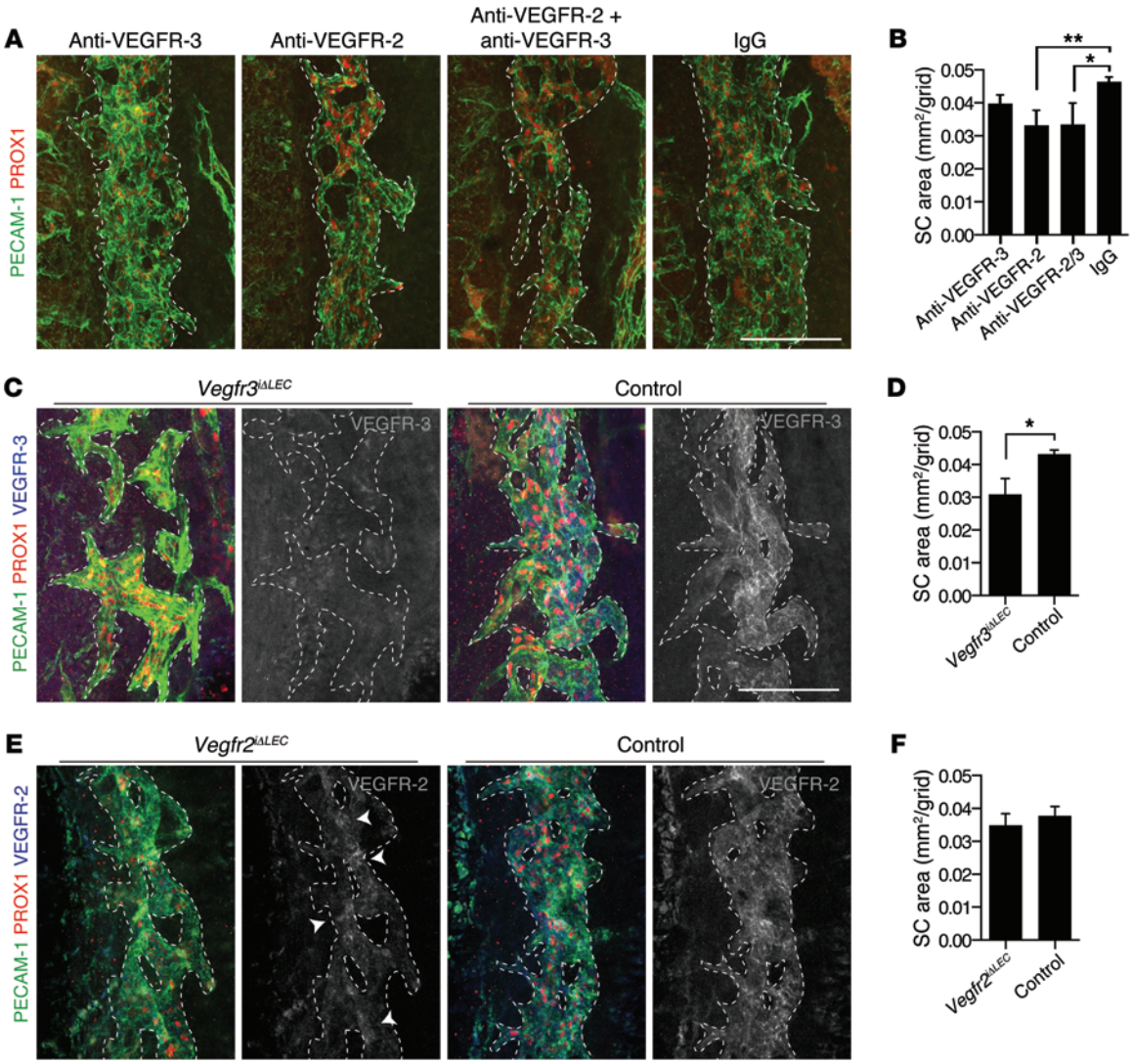

Figure 4. The lymphangiogenic receptor VEGFR-3 is essential for SC development. (**A** and **B**) SC morphology (**A**) and area (**B**; data from 1 litter) after injection of rat anti–VEGFR-3 antibodies (n = 4), rat anti–VEGFR-2 antibodies (n = 4), their combination (n = 3), or control rat IgG (n = 3) once daily during P0–P7 into littermate mice. (**C** and **D**) SC morphology (**C**) and mean area (**D**; data from 1 litter) in *Vegfr3*$^{i\Delta LEC}$ and littermate control *Vegfr3*$^{fl/fl}$ mice (n = 3 per group) at P7 after induction of Cre activity. *Vegfr3* deletion was confirmed using antibodies against VEGFR-3. (**E** and **F**) SC morphology (**E**) and mean area (**F**; data pooled from 2 litters) in *Vegfr2*$^{i\Delta LEC}$ and littermate control *Vegfr2*$^{fl/fl}$ mice (n = 4 per group) mice at P7. *Vegfr2* deletion was confirmed using antibodies against VEGFR-2. Arrowhead indicates residual VEGFR-2. Scale bars: 100 μm (**A**, **C**, and **E**). *P < 0.05; **P < 0.01.

expressing a soluble ligand-binding VEGFR-3 (*K14-VEGFR-3*$_{1-3}$*-Ig*; ref. 26), and mice expressing a soluble non–ligand-binding VEGFR-3 (*K14-VEGFR-3*$_{4-7}$*-Ig*; ref. 35).

During embryogenesis, VEGF-C is expressed predominantly in regions where the lymphatic vessels develop (24). In *Vegfc*$^{+/LacZ}$ mice, in which *LacZ* encoding β-galactosidase has been inserted into the *Vegfc* locus, X-gal staining revealed prominent VEGF-C expression adjacent to the SC. However, despite the total lack of ES lymphatic vasculature in the *Vegfc*$^{+/LacZ}$ heterozygous pups that still expressed VEGF-C, the SC appeared normal at P12 compared with WT littermates (Supplemental Figure 7).

When SC morphology was assessed at P7 in the transgenic mice expressing soluble VEGFR-3 fusion proteins, *K14-VEGFR-3*$_{1-3}$*-Ig* mice were distinguished from their WT littermates and *K14-VEGFR-3*$_{4-7}$*-Ig* control mice by their markedly hypoplastic SC, characterized by lacunae that were disconnected from each other and by reduced SC surface area (Figure 3, A and B).

Both VEGF-C and VEGF-D are neutralized by the *K14-VEGFR-3*$_{1-3}$*-Ig* transgene–encoded protein. To dissect which of the 2 growth factors is required for SC development, we analyzed *Vegfd*$^{-/-}$ mice and *Vegfc*$^{i\Delta R26}$ mice, which were conditionally deleted of *Vegfc* using the *Rosa26-CreER*^{T2} allele that globally expresses a tamoxifen-activated Cre recombinase. SC development in the *Vegfd*$^{-/-}$ pups was not altered (Figure 3, C and D). However, when the SC morphology was assessed after daily 4-OHT injections (from P1 to P5) in *Vegfc*$^{i\Delta R26}$ mice at P7, abnormal hypoplastic SC morphology and reduced SC surface area was observed (Figure 3, E and F), reminiscent of the SC in *K14-VEGFR-3*$_{1-3}$*-Ig* mice.

To assess whether *Vegfd* can compensate for the loss of *Vegfc*, we analyzed *Vegfc*$^{i\Delta R26}$ *Vegfd*$^{-/-}$ double-knockout mice. A

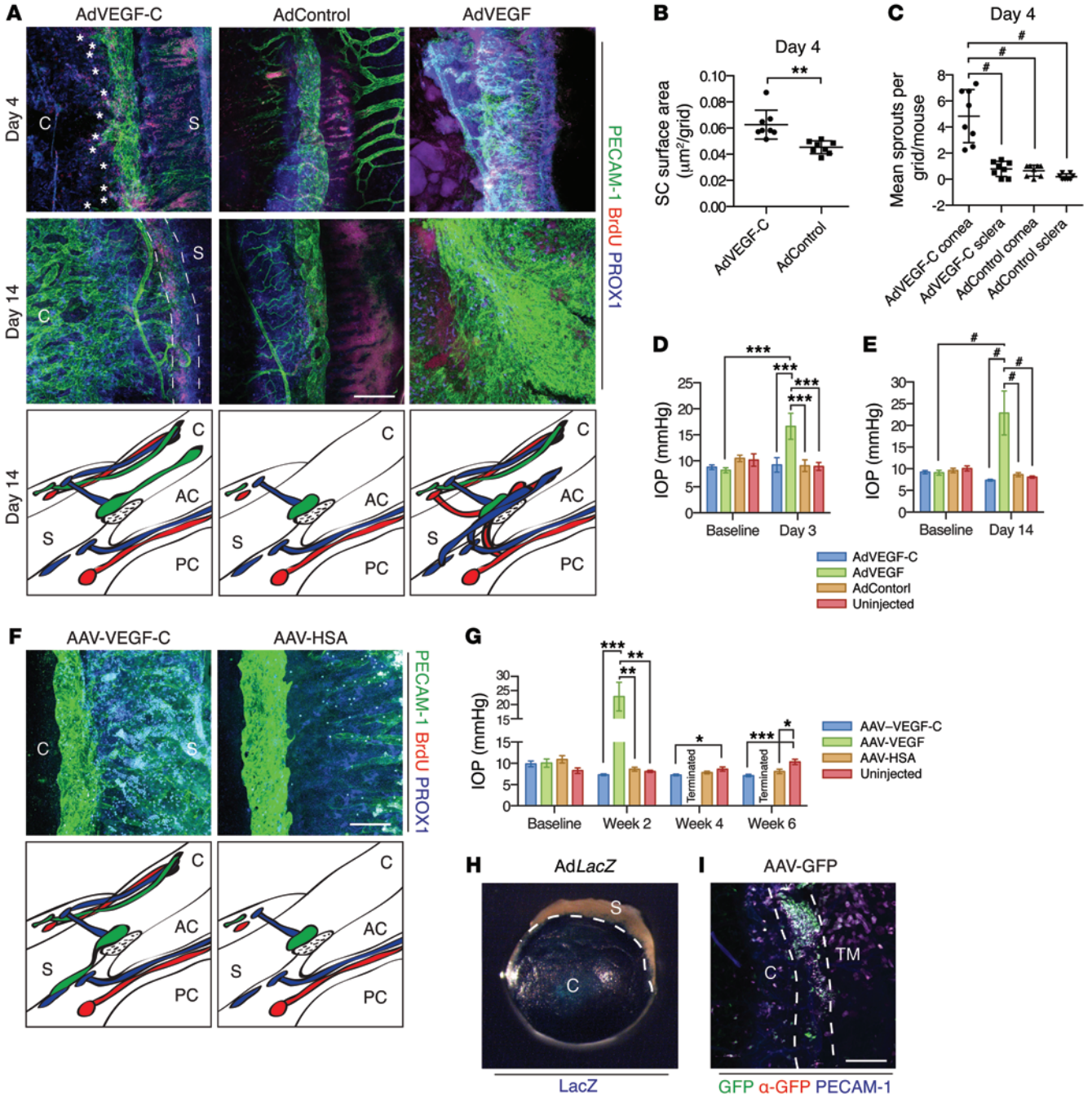

Figure 5. VEGF-C overexpression induces directional sprouting, proliferation, and migration of SC ECs in adults. (**A**–**E**) AdVEGF-C, AdVEGF, or an AdControl was injected into the anterior chamber, as indicated. (**A**) Immunofluorescence staining of the SC with antibodies against PECAM-1 (green), BrdU (red), and PROX1 (blue) at days 4 and 14 after injection. Mice were injected with 100 mg/kg BrdU 2 hours prior to sacrifice. Sprouts of SC ECs (asterisks) are indicated. Changes in limbal vascular anatomy on day 14 are illustrated. C, cornea; S, sclera; AC, anterior chamber; PC, posterior chamber. (**B** and **C**) Quantitative analysis of SC area (**B**) and SC sprouts extending toward the cornea or sclera (**C**). Each symbol represents data from 1 eye. (**D** and **E**) IOP before and 3 (**D**) and 14 (**E**) days after injection. (**F** and **G**) AAV–VEGF-C or AAV-HSA was injected into the anterior chamber. (**F**) Immunofluorescence staining of the SC with indicated antibodies at week 6 after transduction, and illustration of changes in limbal vascular anatomy. (**G**) IOP before and after injection. (**H**) X-gal staining in mice injected with Ad*LacZ*. (**I**) Immunofluorescence in mice injected with reporter AAV vectors encoding EGFP and staining with antibodies against GFP (red) and PECAM-1 (blue). Scale bars: 200 μm (**A**, **F**, and **I**). $^{*}P < 0.05$; $^{**}P < 0.01$; $^{***}P < 0.001$; $^{\#}P < 0.0001$.

trend toward smaller SC surface area was detected in *Vegfc*$^{i\Delta R26}$ *Vegfd*$^{-/-}$ compared with *Vegfc*$^{i\Delta R26}$ eyes, but this was not statistically significant, although the SC sometimes appeared thinner with the compound deletion (Figure 3, G and H).

The lymphangiogenic receptor VEGFR-3 is essential for SC development. VEGFR-3 tyrosine kinase activity is essential for lymphatic vessel growth (21). VEGFR-3 is activated by VEGF-C and VEGF-D, and VEGFR-3 mutations in both mice and in patients

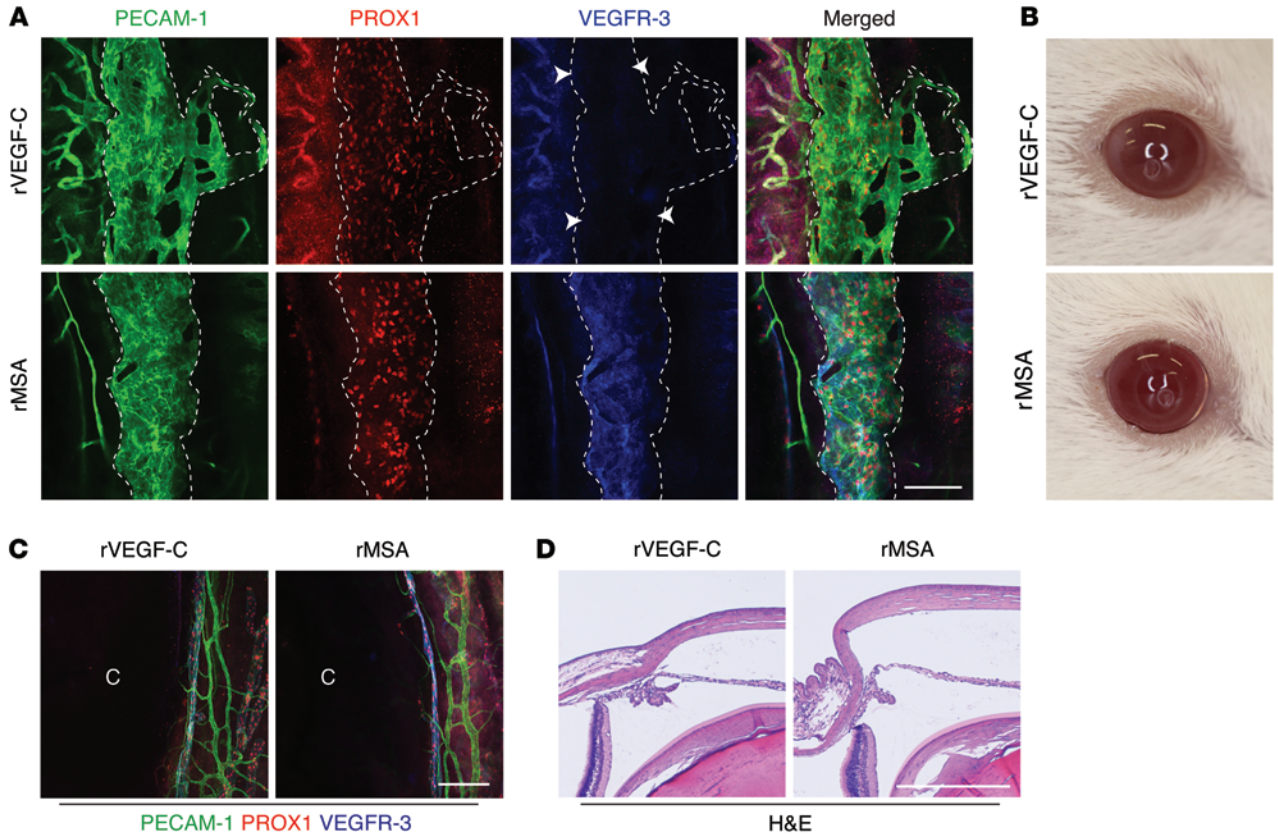

Figure 6. A single injection of rVEGF-C induces enlargement of the SC without corneal neovascularization in adult mice. Mice received a single injection of 3.8 μg rVEGF-C or rMSA. (**A**) Immunofluorescence staining of the SC on day 14 after injection. Dashed outlines denote the SC. rVEGF-C administration showed downregulation of VEGFR-3 by SC ECs (arrowheads). (**B**) Representative macroscopic images of eyes on day 9 after injection, after IOP measurement. (**C**) Corneal and ES vasculature on day 14 after injection. (**D**) Representative images of H&E-stained paraffin-embedded eye sections on day 14. Scale bars: 100 μm (**A** and **C**), 400 μm (**D**).

with Milroy's disease (OMIM 153100) lead to defective development of the lymphatic vasculature, resulting in lymphedema (20). The role of VEGFR-3 signaling in SC development was assessed in *Chy* mice (36), a genetic model of Milroy's disease with a heterozygous kinase-inactivating point mutation in the VEGFR-3 tyrosine kinase domain; in mice administered with VEGFR-2– and VEGFR-3–blocking monoclonal antibodies (*DC101* and *mF4-31C*, respectively; ref. 37); and in mice in which *Vegfr3* or *Vegfr2* was conditionally deleted using a LEC-specific inducible Cre line (*Vegfr3*$^{fl/fl}$ *Prox1-CreER*^{T2} and *Vegfr2*$^{fl/fl}$ *Prox1-CreER*^{T2}; referred to herein as *Vegfr3*$^{i\Delta LEC}$ and *Vegfr2*$^{i\Delta LEC}$, respectively, refs. 31, 38, 39).

In the *Chy* mice, lack of ES lymphatic vasculature was observed, similar to that in the *Vegfc* heterozygous mice. However, as in *Vegfc*$^{+/LacZ}$ mice, no defects were observed in the SC by immunofluorescence at P12 (Supplemental Figure 8). When VEGFR-2, VEGFR-3, or the combination of VEGFR-2 and VEGFR-3 blocking antibodies were administered daily from P0 to P6, SC hypoplasia was detected most significantly in the anti–VEGFR-2– and anti–VEGFR-2/3–treated mice at P7, whereas blocking VEGFR-3 did not lead to a statistically significant reduction in SC area; furthermore, no additive effects were detected when both VEGFR-3 and VEGFR-2 antibodies were used (Figure 4, A and B). The discrepancy between the effect of *Vegfc* deletion and VEGFR-3 blocking antibodies lead us to hypothesize that the antibodies had reduced bioavailability in the SC due to blood-eye barrier development and SC transition to a blind-ended tube. Indeed, our data indicated that between P3 and P4, before induction of VEGFR-3 expression in SC ECs, the SC was no longer perfused by blood (Supplemental Figure 4, U–X). VEGFR-2 expression was also detected in the earliest stages of SC development (Supplemental Figure 4, A–T), which suggests that the early stages of SC development involve VEGFR-2 but not VEGFR-3 signaling.

The functional importance of VEGFR-3 and VEGFR-2 in later SC development was examined with lymphatic-specific deletion of *Vegfr3* or *Vegfr2*, starting around P2, when PROX1 is induced. The resulting *Vegfr3*$^{i\Delta LEC}$ and *Vegfr2*$^{i\Delta LEC}$ phenotypes thus reflect receptor functions at later stages of development. Induction of Cre activity in *Vegfr3*$^{i\Delta LEC}$ mice by daily 4-OHT injections from P1 to P5 resulted in a markedly hypoplastic SC with reduced surface area at P7 compared with control littermates, indicative of a critical role of VEGFR-3 in SC development. *Vegfr3*$^{i\Delta LEC}$ mice were characterized by SC lacunae that failed to connect with each other, similar to the *K14-VEGFR-3*$_{1-3}$*-Ig* and *Vegfr2*$^{i\Delta LEC}$ mice, and no residual VEGFR-3 staining was detected (Figure 4, C and D). The SC appeared normal in the 4-OHT–treated *Vegfr2*$^{i\Delta LEC}$ mice (Figure 4, E and F), although *Vegfr2* gene deletion was somewhat incomplete.

VEGF-C overexpression induces directional sprouting, proliferation, and migration of SC ECs in adults. VEGF-C has been shown to

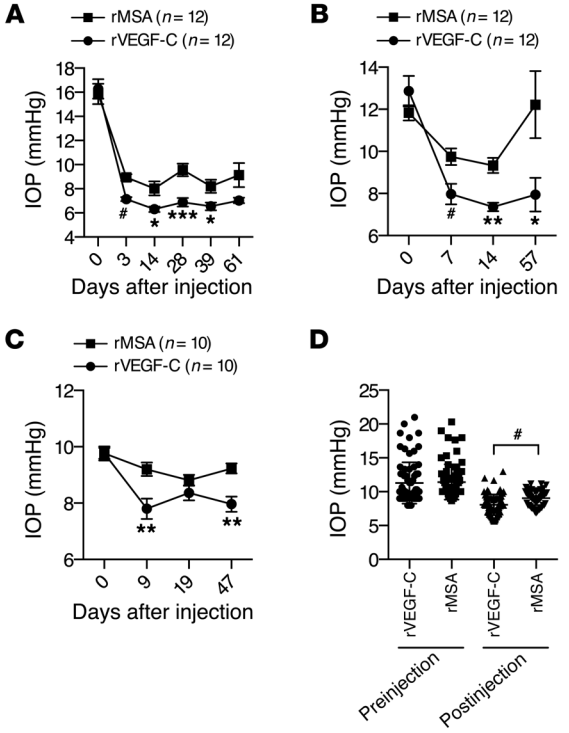

Figure 7. A single injection of recombinant VEGF-C is associated with a sustained decrease in IOP in adult mice. (**A**–**C**) IOP after injection of rVEGF-C or rMSA into the anterior chamber of aged (**A**, 43 weeks; **B**, 41 weeks) or young (**C**, 7 weeks) mice. 9.6 μg protein was injected in 4 μl. A substantial proportion of the injected fluid was backflushed. Age-controlled female NMRI mice were used. (**D**) Meta-analysis of all IOP experiments performed (see **A**–**C** and Supplemental Figure 11 for individual experiments). All postinjection IOP measurements from 1 eye were averaged. Postinjection *t* test: rVEGF-C, 8.153 ± 0.1711 mmHg, n = 84; rMSA, 9.239 ± 0.1341 mmHg, n = 81; difference, 1.086 ± 0.2184; 95% CI, 0.6543 to 1.517; R^2 = 0.1316. $^*P < 0.05$; $^{**}P < 0.01$; $^{***}P < 0.001$; $^{\#}P < 0.0001$.

induce sprouting, proliferation, migration, and survival of LECs, both in vitro and in vivo in adults (20, 27, 28). The role of VEGF-C/VEGFR-3 signaling in SC development led us to hypothesize that VEGF-C could be used for therapeutic manipulation of the SC in order to facilitate AH outflow in the treatment of glaucoma. To provide initial proof of principle, we first analyzed the effects of VEGF-C or VEGF overexpression in the anterior segment of the eye by using viral vectors.

Adenoviral vectors encoding VEGF-C (AdVEGF-C) or VEGF165 (AdVEGF), or an empty control vector (AdControl), were injected into the anterior chamber of NMRI *nu/nu* mouse eyes. To assess effects on aqueous outflow facility, IOP measurements were performed before injection and before sacrifice. The effects of VEGF-C and VEGF overexpression on SC ECs were studied in whole-mount eyes stained for PECAM-1 and PROX1. To identify proliferating ECs, mice received an injection of BrdU 2 hours prior to sacrifice, and the BrdU incorporated to nuclear DNA was stained. At day 4, marked sprouting and proliferation of SC ECs was detected in VEGF-C–treated eyes (Figure 5A). VEGF-C treatment was associated with an increase in SC surface area, and sprouts from the SC extended almost exclusively toward the inner surface of the cornea (Figure 5, A–C). Surprisingly, by 2 weeks, large areas of the cornea were filled with PROX1-positive SC ECs connected to the original circular SC. Explaining the corneal involvement, β-galactosidase staining revealed effective transfection of the cornea when the adenoviral reporter vector encoding β-galactosidase (Ad*LacZ*) was used (Figure 5H). In striking contrast, AdVEGF treatment entirely obliterated the aqueous outflow system at day 4, and by day 14, only a sheet of ECs surrounding the limbus could be detected (Figure 5A). Furthermore, treatment with AdVEGF was associated with a marked increase in IOP, resembling neovascular glaucoma (40). On the other hand, AdVEGF-C–treated eyes had normal IOP compared with AdControl-injected and uninjected eyes at day 4 as well as a trend toward lower IOP at day 14, albeit not statistically significant (Figure 2, D and E).

To study the effects of long-term VEGF-C overexpression, adeno-associated viral vectors (AAVs) encoding VEGF-C, VEGF, or human serum albumin (HSA) were injected into the anterior chamber of NMRI *nu/nu* mice, and eyes were analyzed 6 weeks after transduction. Surprisingly, AAV–VEGF-C injection resulted in the extension of PROX1-positive SC outpockets toward the sclera (Figure 5F), in the opposite direction of that observed in AdVEGF-C–injected eyes. Although ocular puncture and/or AAV administration by itself resulted in decreased IOP, AAV–VEGF-C induced a more significant decrease of IOP compared with AAV-HSA–injected or uninjected eyes (Figure 5G). In striking contrast, AAV-VEGF administration in equal viral particle amounts resulted in the obliteration of the eye (data not shown), associated with massive increases in IOP, forcing an early sacrifice after 2 weeks (Figure 5G). To explain preferential scleral growth of the SC, mice injected with AAVs encoding enhanced GFP (EGFP) were analyzed. Immunofluorescence and anti-GFP staining revealed preferential AAV expression in limbal cells and in cells on the scleral side of the SC (Figure 5I).

A single intraocular injection of recombinant VEGF-C induces SC enlargement associated with a trend of decreasing IOP. In order to study the potential of VEGF-C in inducing therapeutic growth of the SC for the reduction of IOP, we studied aged NMRI mice to model the aging-associated changes in the eye that may underline glaucoma, and applied recombinant VEGF-C in order to avoid potential detrimental effects of sustained protein production via viral vectors (Supplemental Figure 9, A–C). First, to provide proof of principle that recombinant VEGF-C (rVEGF-C) induces SC growth, rVEGF-C, rVEGF, or HSA was injected into the anterior chamber on 3 consecutive days. Upon analysis at day 4, rVEGF-C–induced proliferation and sprouting of SC ECs was observed preferentially toward the sclera, whereas rVEGF obliterated the vascular aqueous outflow system (Supplemental Figure 10). While rVEGF induced massive corneal angiogenesis, only mild activation of ES blood vessels was observed in rVEGF-C–injected eyes (Supplemental Figure 9D). To overcome potential corneal neovascularization and to study the effects of rVEGF-C on aqueous outflow, we further lowered the dose to a single injection of 0.264, 3.8, 6.4, or 9.6 μg rVEGF-C. As a control, we used recombinant mouse serum albumin (rMSA) produced and purified by the same method. By whole-mount immunofluorescence, rVEGF-C treatment was observed to induce mild but clear growth of the SC toward the sclera (Figure 6A). Macroscopically, all rVEGF-C–injected eyes appeared normal (Figure 6B). Moreover, rVEGF-C

did not induce any corneal neovascularization, and no pathological changes were detected in H&E staining of rVEGF-C–injected eyes at 2 weeks (Figure 6, C and D). Although ocular puncture decreased IOP by itself, rVEGF-C resulted in variable, but often sustained, IOP decrease when using several separate protein lots (Figure 7, A–C, and Supplemental Figure 11). In meta-analysis of all experiments, the postinjection average IOP of rVEGF-C–treated eyes was lower (rVEGF-C, 8.153 ± 0.1711 mmHg, $n = 84$; rMSA, 9.239 ± 0.1341 mmHg, $n = 81$; difference, 1.086 ± 0.2184; 95% CI, 0.6543 to 1.517; $P < 0.0001$; Figure 7D). Despite the variation in the results, the trend toward lowering of the IOP suggested that a single injection of low-dose rVEGF-C could safely induce SC growth and sustained IOP decrease.

Discussion

In the present study, we established the SC as lymphatic-like vessel that displays many, but not all, features of terminally differentiated lymphatic endothelium. We showed expression of PROX1 by SC ECs in humans, zebrafish, and mice, which indicates that the lymphatic-like identity of the SC is conserved in vertebrate evolution. In mice, SC ECs expressed PROX1, VEGFR-3, CCL21, Itga9, and collagen IV and had no surrounding pericytes or vascular smooth muscle cells, similar to lymphatic capillaries. Moreover, SC ECs were FOXC2$^{-/lo}$ and characterized by zipper-type interendothelial junctions. However, SC ECs were distinguished from lymphatic endothelium by stronger PECAM-1 expression, little or no LYVE-1 expression, and lack of podoplanin expression.

We demonstrated that the development of the SC occurred in a manner similar to, yet distinct from, the development of the lymph sacs (Supplemental Figure 12 and ref. 23). SC morphogenesis begins when limbal transcleral veins begin to sprout laterally, form strings of ECs mimicking the strings of initial LECs that connect each other, and coalesce into a primordial SC analogous to the primordial thoracic duct. Unlike in the cardinal veins, where PROX1 is induced in a subset of the venous ECs (24), PROX1 was induced in the SC only after the initial formation of a primordial SC. If SC ECs are defined as truly lymphatic, SC development would represent an exception to the concept that all LECs are derived from lymph sacs (22). This would also be an exception to the concept that all lymphatic vessels drain into systemic circulation via the thoracic duct and the right lymphatic duct.

The VEGF-C/VEGFR-3 pathway is the first critical pathway described for the development of the lymphatic vascular tree. VEGFR-3 is activated by VEGF-C and VEGF-D, both members of VEGF family of growth factors (21). In developing lymphatic vessels, VEGF-C is required for the migration of PROX1-expressing initial LECs (23, 24). In *Vegfc*$^{-/-}$ mice, PROX1-positive cells committed to the lymphatic lineage are initially seen in the common cardinal veins and the superficial venous plexus, but they fail to migrate to form the primordial thoracic duct and the primordial longitudinal lymphatic vessel (collectively the lymph sacs) (23). In *Vegfc*$^{+/-}$ mice, lymph sacs are detected, but they display subsequent defects, leading to hypoplastic lymphatics and lymphedema (24). We showed here that conditional VEGF-C deletion (*Vegfc*^{iAR26} mice) inhibited SC development. However, even in the absence of both VEGF-C and VEGF-D, the SC could develop, although it was markedly hypoplastic. These differences may reflect the fact that SC ECs differentiate into lymphatic-like lineage only after a primordial SC has formed, whereas embryonic LEC progenitors differentiate into LECs while still residing in the cardinal vein. Although the mouse model for Milroy's disease did not show SC defects, by conditionally deleting *Vegfr3* in SC ECs, we demonstrated a critical role for VEGFR-3 in SC development. Furthermore, we showed that at least the initial stages of SC development involve VEGFR-2, as it was expressed in the initial transscleral vessels and throughout SC development, and its blocking with monoclonal antibodies inhibited SC growth. Thus, the initial stages of SC development appear to be driven by VEGFR-2, but later, after PROX1 and VEGFR-3 induction, VEGFR-3 becomes dominant in driving SC maturation. According to this, patients with Milroy's disease are not likely to have AH outflow defects; indeed, to date, there have been no reports of excess glaucoma among such patients. However, bilateral congenital glaucoma is rarely seen in Hennekam syndrome, which may be due to SC developmental defects, as the responsible mutant gene product, CCBE1, is involved in VEGF-C cleavage into its active form (41).

Prompted by these findings, we conducted experiments in adult mice to show that VEGF-C overexpression in the anterior chamber of the eye results in the sprouting, proliferation, and migration of SC ECs with a trend toward IOP reduction. VEGF, on the other hand, which is upregulated in neovascular glaucoma, obliterated the AH drainage system. To account for this difference, we show that VEGFR-2 was expressed in all vessels around the limbus, whereas VEGFR-3 expression was restricted to SC ECs and ES lymphatic vessels (see Supplemental Figure 13). Most strikingly, a single injection of recombinant VEGF-C induced mild SC lymphangiogenesis without inducing corneal neovascularization or other pathologies, showing a trend toward surprisingly sustained IOP decrease. The relatively modest effect on IOP may be related to differences in the amount of backflush from the 4-μl volume injected into the anterior chamber. Additionally, in mice (unlike in humans), about 80% of the AH outflow does not flow through the SC (42). These results suggest dramatically opposing roles of VEGF and VEGF-C in the regulation of AH outflow.

In conclusion, our findings may open novel therapeutic avenues for the treatment of glaucoma. Regardless of whether SC ECs are lymphatic, the relatively selective expression of VEGFR-3 and other PROX1 downstream genes may be exploited in glaucoma treatment to specifically modulate SC function, with minimal blood vascular and other side effects. Regarding the potential therapeutic use of rVEGF-C in the treatment of glaucoma, further studies in rabbits and primates are warranted, due to species differences in the AH outflow system and ocular anatomy.

Methods

Antibodies. The following primary antibodies were used for immunostaining of mouse tissues: rabbit anti-mouse PROX1 (diluted 1:200; ref. 43), goat anti-human PROX1 (diluted 1:500; AF2727, R&D Systems), polyclonal goat anti-mouse VEGFR-3 (diluted 1:100; AF743, R&D Systems), goat anti-mouse VEGFR-2 (diluted 1:100; AF644, R&D Systems), unconjugated rat anti–PECAM-1 (diluted 1:500; clone MEC 13.3, 553370, BD Biosciences — Pharmingen), hamster anti–PECAM-1 (diluted 1:500; clone 2H8, MAB1398Z, Chemicon), Cy3-conjugated mouse anti-SMA (clone 1A4, C6189, Sigma-Aldrich), polyclonal rabbit

anti–LYVE-1 (diluted 1:1,000; ref. 24), goat anti-CCL21 (diluted 1:100; AF457, R&D Systems), VE-cadherin (diluted 1:100; clone 11D4.1, BD Biosciences — Pharmingen), rabbit anti-mouse collagen IV (diluted 1:1,000; LB-1403, Cosmo Bio), rabbit polyclonal anti-GFP (diluted 1:1,000; TP401, Torrey Pines Biolabs), rabbit anti-NG2 (diluted 1:500; AB5320, Millipore), IgG fraction of rabbit polyclonal anti-mouse podoplanin (diluted 1:200, provided by D. Kerjaschki, Medical University of Vienna; ref. 44), goat polyclonal anti–integrin α9 (diluted 1:500; AF3827, R&D Systems), rat anti-FOXC2 (diluted 1:2,500; ref. 45). The primary antibodies were detected with the appropriate Alexa Fluor 488, Alexa Fluor 594, Alexa Fluor 633 or Alexa Fluor 647 secondary antibody conjugates (diluted 1:500; Molecular Probes/Invitrogen). BrdU was detected with Alexa Fluor 594–conjugated mouse anti-BrdU antibodies (diluted 1:500; Molecular Probes/Invitrogen) after incubation in hydrochloric acid and neutralization using sodium tetraborate. For staining in human sections, biotinylated rabbit anti-goat IgG (diluted 1:300; BA-5000, Vector Laboratories) antibody was used.

Generation of Vegfc gene targeted mice. *Vegfc*^{iAR26} mice were created by inserting a LoxP-flanked mouse *Vegfc* cDNA and a Frt-flanked Neo cassette into the first exon of the mouse *Vegfc* genomic locus, before the translation initiation codon, leaving an intact coding sequence for *Vegfc* while deleting 137 bp of the first intron of the *Vegfc* gene. See Supplemental Methods for details.

Mice and tissues. The mouse lines *Sox18-CreER*^{T2} (32), *Vegfc*$^{+/LacZ}$ (24), *K14-VEGFR-3*$_{1-3}$*-Ig* (26), *K14-VEGFR-3*$_{4-7}$*-Ig* (35), *Vegfd*$^{-/-}$ (34), *Chy* (36), *Vegfr3*$^{fl/fl}$ (38), *Vegfr2*$^{fl/fl}$ (provided by R. Adams, Max Planck Institute for Molecular Biomedicine; ref. 39), *Rosa26-CreER*^{T2} (33), *Prox1-CreER*^{T2} (31), *Rosa26*^{mTmG} (46), and *LSL-tdTomato* (30) have been described previously. NMRI, NMRI *nu/nu*, and albino B6 mice were used for the experiments. Genetic strains were in the C57BL/6J background, with the exception of *Vegfc*$^{+/LacZ}$ (ICR) and *Chy* and *Vegfd*$^{-/-}$ (NMRI). *Vegfc*$^{fl/fl}$ mice were in a mixed C57BL/6J and 129SV background, and *Vegfc*$^{fl/fl}$ *Vegfd*$^{-/-}$ mice in a mixed C57BL/6J, 129SV, and NMRI background; both were backcrossed at least 6 generations into the C57BL/6J background. For the induction of Cre-mediated recombination in neonatal *Vegfr3*^{iΔLEC}, *Vegfr2*^{iΔLEC}, *Vegfc*^{iΔR26}, or control mice, 2 μl 4-OHT (25 mg/ml dissolved in ethanol) was injected intragastrically using a 10-μl Hamilton syringe. Daily injections were performed from P0 or P1 to P6, and vessels were analyzed at P7. Deletion efficacy was validated either by staining (*Vegfr3*$^{fl/fl}$ and *Vegfr2*$^{fl/fl}$) or by RT-qPCR (*Vegfc*$^{fl/fl}$; see Supplemental Methods). For genetic lineage tracing, 4-OHT was injected intraperitoneally at P0 or at P0 and P4, and vessels were analyzed at P7. For *Sox18-CreER*^{T2} lineage tracing, 4-OHT was injected at P2, P3, and P4, and vessels were analyzed at P7. After sacrificing the mice, tissues were immersed in 4% paraformaldehyde, washed in PBS, and then processed for whole-mount staining.

Zebrafish eyes were provided by P. Panula (University of Helsinki).

Human samples. Eyes that had been enucleated due to uveal melanoma were found through the registry of the Ophthalmic Pathology Laboratory of Helsinki University Eye Hospital and provided by T. Kivelä (Helsinki University Central Hospital). 2 formalin-fixed, paraffin-embedded eyes without tumor extension to the ciliary body or glaucoma were selected for analysis.

Generation and in vitro analysis of viral vectors. The adenoviral vectors encoding VEGF-C, VEGF165, LacZ, and the empty CMV (provided by S. Ylä-Herttuala, University of Eastern Finland, Kuopio, Finland), and the adeno-associated viral (AAV) constructs encoding VEGF-C, VEGF165, HSA, and EGFP, were produced and analyzed as described previously (24, 27, 47–49).

Protein expression and purification. Full-length human VEGF-C (residues 32–419; ref. 41) and mouse albumin (residues 25–608) were cloned into the pFastBac1 (Invitrogen) baculovirus expression vector with mellitin signal peptide and a C-terminal hexahistidine tag. Recombinant baculovirus was produced in *Spodoptera frugiperda* (Sf9) insect cells grown at +26°C in serum-free Insect-Express (Lonza) medium. For protein expression, *Trichoplusia ni* (Tn5) insect cells were grown in about 250 ml serum-free Insect-Express (Lonza) medium per 1-l shaker flask at +26°C and 110 rpm shaker speed. The cell cultures were infected with the corresponding recombinant baculovirus at high multiplicity, and at 3 days after infection, the supernatant was harvested by centrifugation for 20 minutes at 8,000 *g*.

The supernatant was supplemented with 10 mM imidazole and 2 mM $NiCl_2$ and was loaded onto Ni^{2+}-charged resin (Ni-NTA Superflow; Qiagen) column with a peristaltic pump. The resin was extensively washed with 20 mM HEPES (pH 7.5) containing 20 mM imidazole and 0.6 M NaCl. The target proteins were eluted with the washing buffer supplemented with 0.4 M imidazole. Mouse albumin was further purified by gel filtration on a Superdex 200 (GE Healthcare) column in PBS and brought to the desired concentration by centrifugal filter units (Amicon Ultra-15 MWCO 10 kDa; Millipore). For VEGF-C purification, the Ni^{2+} affinity step was repeated by reloading the eluate in 20 mM HEPES (pH 7.5) containing 20 mM imidazole and 0.6 M NaCl. The buffer was changed to PBS, and the protein was brought to the desired concentration by centrifugal filter units at room temperature (RT).

IOP measurement. IOP was measured with an induction/impact tonometer (Icare TONOLAB; Icare Finland) (50) that was mounted to a stand and clamp according to the manufacturer's recommendation. After the mice were anesthetized with intraperitoneally administered ketamine (60 mg/kg; Ketaminol Vet, Intervet International B.V.) and xylazine (6 mg/kg; Rompun Vet, KVP Pharma + Veterinär Produkte GmbH), they were placed on an adjustable-height platform. The position of the mouse and the platform were adjusted so that the apex of the central cornea was normal to and 2–3 mm away from the probe tip. The digital readout of 6 consecutive IOP measurements was obtained from the tonometer in mm Hg. This was repeated 3 times for each eye. The mean of the 3 readouts was used in the analysis. Repeat IOP measurements were performed at the same time of day as the baseline measurements in order to avoid circadian fluctuations in the readings (51).

Intraocular injection. After baseline IOP measurements, intraocular injection of the indicated preparations was performed with a 30-gauge, 0.5-inch needle (BD Microlance 3; BD Drogheda) attached to a 10-μl Hamilton microliter syringe (Model 701 LT SYR; Hamilton Co.). The needle was inserted into the anterior chamber 1 mm posterior from the limbus and into the 10:30 clock position in order to avoid larger blood vessels. The needle was inserted through the posterior chamber into the pupil, where the protein was injected. For the recombinant proteins, 0.264, 3.8, 6.4, or 9.6 μg protein was injected. For adenoviral vectors, 5.80×10^7 pfu was injected. For AAVs, 3.38×10^9 viral particles were injected.

Immunostaining, X-gal staining, BrdU staining, and microscopy. For whole-mount staining, the fixed anterior segment of the eye was separated in a coronal plane. The retina and lens were removed. The tissues were permeabilized in 0.3% Triton X-100 in PBS (PBS-TX) and blocked in 5% donkey serum. Primary antibodies were added

to the blocking buffer and incubated with the tissue overnight at RT. After washes in PBS-TX, the tissue was incubated with fluorophore-conjugated secondary antibodies in PBS-TX overnight at RT, followed by washing in PBS-TX. After postfixation in 1% PFA, the tissues were washed with PBS, cut into 4 quadrants, and mounted. For thick cryosections, 50-μm eye sections were air-dried, encircled with a pappen, fixed in 4% PFA for 8 minutes, rehydrated in PBS, and blocked with 3% BSA in PBS-TX at RT. After primary antibody incubation at +4°C in 3% BSA in PBS overnight, sections were washed with PBS and incubated for 2–3 hours with the appropriate fluorophore-conjugated secondary antibody conjugates (diluted 1:300) in 3% BSA in PBS. After washes with 0.1% PBS-TX, sections were mounted. All fluorescently labeled samples were mounted with Vectashield mounting medium containing DAPI (H-1200; Vector Laboratories). For visualization of VEGF-C expression in *Vegfc*$^{+/LacZ}$ reporter mice, tissues were fixed with 0.2% glutaraldehyde and stained by the β-galactosidase substrate X-Gal (Promega). For BrdU stainings, mice were given 100 mg/kg BrdU by intraperitoneal injection 2 hours before sacrifice. For tyramide signal amplification immunohistochemistry of human sections, see Supplemental Methods.

Microscopy. Fluorescently labeled samples were analyzed with a confocal microscope (Zeiss LSM 510 Meta, objectives ×10 with NA 0.45 and oil objectives ×40 with NA 1.3; Zeiss LSM 5 Duo, objectives ×10 with NA 0.45 and oil objective ×40 with NA 1.3, and Zeiss LSM 780, objectives ×10 with NA 0.45, ×20 with NA 0.80, oil objective ×40 with NA 1.3) using multichannel scanning in frame mode, as described previously (37). The pinhole diameter was set at 1 Airy unit for detection of the Alexa Fluor 488 signal and was adjusted for identical optical slice thickness for the fluorophores emitting at higher wavelengths. Zeiss ZEN 2010 or LSM AIM (release 4.2) software was used for image acquisition. 3D projections were digitally reconstructed from confocal *z* stacks. 3D volume renderings and videos were generated with Imaris software (Bitplane). Brightfield microscopy was performed with a Leica DM LB microscope (objectives ×10 with NA 0.25 and ×20 with NA 0.4) with an Olympus DP50 color camera. Images were edited using Image J or Adobe Photoshop software.

Morphometric and quantitative vessel analysis. The vascular surface areas of the SC were quantified as PECAM-1–positive area from confocal micrographs acquired of all intact quarters of the anterior segment using Image J software. For statistical analysis, the surface areas from 3–4 quadrants were averaged from one or both eyes.

Statistics. Quantitative data were compared between groups by 2-sample (unpaired Student's) 2-tailed *t* test assuming equal variance, or 1- or 2-way ANOVA followed by Tukey post-hoc test for multiple comparisons. Values are expressed as mean ± SD, except in graphs (mean ± SEM). A *P* value less than 0.05 was considered significant.

Study approval. All animal experiments were approved by the Committee for Animal Experiments of the District of Southern Finland and conformed to the Association for Research in Vision and Ophthalmology Statement for the Use of Animals in Ophthalmic and Vision Research. Informed consent for human material from the pathology archive was not required because tissue had been excised and originally processed as a routine diagnostic procedure.

Acknowledgments

We thank M. Robciuc, W. Zheng, K. Heinolainen, G. D'Amico Lago, and A. Anisimov (University of Helsinki) for support and advice; M. Jeltsch for generating the rhVEGFC construct; A. Nagy (Mount Sinai Hospital) and R. Adams for the *Vegfr2*$^{fl/fl}$ mice; T. Kivelä for providing human eye sections; R. Skoczylas (University of Queensland) for *Sox18-CreER*^{T2} reporter eyes; S. Ylä-Herttuala for adenoviruses; D. Kerjaschki for podoplanin antibody; P. Panula for zebrafish eyes; J. Kenkkilä (Biomedicum Imaging Unit) for assistance with confocal microscopy and 3D rendering; G.Y. Koh, D.Y. Park, and J. Lee (KAIST) for helpful discussions; S. Kajander, K. Lintula, K. Salo, K. Mänttäri, J. Koponen, and T. Tainola (University of Helsinki) for technical assistance; and the staff of the University of Helsinki Laboratory Animal Centre for assistance. This study was supported by grants from the Academy of Finland, the Sigrid Juselius Foundation, the European Research Council (ERC-2010-AdG-268804), and the Leducq Foundation (11CVD03). A. Aspelund obtained support from the Finnish Cultural Foundation and the Glaucoma Support Fund Lux. T. Mäkinen obtained funding from Beijer Foundation.

Address correspondence to: Kari Alitalo, Wihuri Research Institute and Translational Cancer Biology Program, Biomedicum Helsinki, University of Helsinki, P.O.B. 63 (Haartmaninkatu 8), 00014 Helsinki, Finland. Phone: 358.9.191.25511; E-mail: kari.alitalo@helsinki.fi.

1. Kwon YH, Fingert JH, Kuehn MH, Alward WLM. Primary open-angle glaucoma. *N Engl J Med*. 2009;360(11):1113–1124.
2. Resnikoff S, et al. Global data on visual impairment in the year 2002. *Bull World Health Organ*. 2004;82(11):844–851.
3. Quigley HA, Broman AT. The number of people with glaucoma worldwide in 2010 and 2020. *Br J Ophthalmol*. 2006;90(3):262–267.
4. Ramos RF, Hoying JB, Witte MH, Daniel Stamer W. Schlemm's canal endothelia, lymphatic, or blood vasculature? *J Glaucoma*. 2007;16(4):391–405.
5. Almasieh M, Wilson AM, Morquette B, Cueva Vargas JL, Di Polo A. The molecular basis of retinal ganglion cell death in glaucoma. *Prog Retin Eye Res*. 2012;31(2):152–181.
6. Boland MV, et al. Comparative effectiveness of treatments for open-angle glaucoma: a systematic review for the U.S. Preventive Services Task Force. *Ann Intern Med*. 2013;158(4):271–279.
7. Kholdebarin R, Campbell RJ, Jin Y-P, Buys YM. Multicenter study of compliance and drop administration in glaucoma. *Can J Ophthalmol*. 2008;43(4):454–461.
8. Schlemm F. Bulbus oculi. In: Th. Chr. Fr. Enslin. *Theoretisch-praktisches Handbuch der Chirurgie, mit Einschluß der syphilitischen und Augen-Krankheiten*. Berlin, Germany; Carl Gerold, Wien; 1830:331–338.
9. Kagemann L, et al. Identification and assessment of Schlemm's canal by spectral-domain optical coherence tomography. *Invest Ophthalmol Vis Sci*. 2010;51(8):4054–4059.
10. Libby RT, et al. Modification of ocular defects in mouse developmental glaucoma models by tyrosinase. *Science*. 2003;299(5612):1578–1581.
11. Perry LP, Jakobiec FA, Zakka FR, Walton DS. Newborn primary congenital glaucoma: histopathologic features of the anterior chamber filtration angle. *J AAPOS*. 2012;16(6):565–568.
12. Smith RS, et al. Haploinsufficiency of the transcription factors FOXC1 and FOXC2 results in aberrant ocular development. *Hum Mol Genet*. 2000;9(7):1021–1032.
13. Fan BJ, Wiggs JL. Glaucoma: genes, phenotypes, and new directions for therapy. *J Clin Invest*. 2010;120(9):3064–3072.
14. Dvorak-Theobald G. Schlemm's canal: its anastomoses and anatomic relations. *Trans Am Ophthalmol Soc*. 1934;32:574–595.
15. Caspi RR. Ocular autoimmunity: the price of privilege? *Immunol Rev*. 2006;213:23–35.
16. Streilein JW. Ocular immune privilege: therapeutic opportunities from an experiment of nature. *Nat Rev Immunol*. 2003;3(11):879–889.
17. Gong H, Tripathi RC, Tripathi BJ. Morphology of the aqueous outflow pathway. *Microsc Res Tech*.

1996;33(4):336–367.
18. Hamanaka T, Bill A, Ichinohasama R, Ishida T. Aspects of the development of Schlemm's canal. *Exp Eye Res*. 1992;55(3):479–488.
19. Leak LV, Burke JF. Ultrastructural studies on the lymphatic anchoring filaments. *J Cell Biol*. 1968;36(1):129–149.
20. Alitalo K. The lymphatic vasculature in disease. *Nat Med*. 2011;17(11):1371–1380.
21. Tammela T, Alitalo K. Lymphangiogenesis: Molecular mechanisms and future promise. *Cell*. 2010;140(4):460–476.
22. Oliver G, Srinivasan RS. Endothelial cell plasticity: how to become and remain a lymphatic endothelial cell. *Development*. 2010;137(3):363–372.
23. Hägerling R, et al. A novel multistep mechanism for initial lymphangiogenesis in mouse embryos based on ultramicroscopy. *EMBO J*. 2013;32(5):629–644.
24. Karkkainen MJ, et al. Vascular endothelial growth factor C is required for sprouting of the first lymphatic vessels from embryonic veins. *Nat Immunol*. 2004;5(1):74–80.
25. Wigle JT, Oliver G. Prox1 function is required for the development of the murine lymphatic system. *Cell*. 1999;98(6):769–778.
26. Makinen T, et al. Inhibition of lymphangiogenesis with resulting lymphedema in transgenic mice expressing soluble VEGF receptor-3. *Nat Med*. 2001;7(2):199–205.
27. Tammela T, et al. Therapeutic differentiation and maturation of lymphatic vessels after lymph node dissection and transplantation. *Nat Med*. 2007;13(12):1458–1466.
28. Lähteenvuo M, et al. Growth factor therapy and autologous lymph node transfer in lymphedema. *Circulation*. 2011;123(6):613–620.
29. Zheng W, Aspelund A, Alitalo K. Lymphangiogenic factors, mechanisms, and applications. *J Clin Invest*. 2014;124(3):878–887.
30. Madisen L, et al. A robust and high-throughput Cre reporting and characterization system for the whole mouse brain. *Nat Neurosci*. 2010;13(1):133–140.
31. Bazigou E, et al. Genes regulating lymphangiogenesis control venous valve formation and maintenance in mice. *J Clin Invest*. 2011;121(8):2984–2992.
32. Coxam B, et al. Pkd1 regulates lymphatic vascular morphogenesis during development. *Cell Rep*. 2014;7(3):623–633.
33. Vooijs M, Jonkers J, Berns A. A highly efficient ligand-regulated Cre recombinase mouse line shows that LoxP recombination is position dependent. *EMBO Rep*. 2001;2(4):292–297.
34. Baldwin ME, et al. Vascular endothelial growth factor D is dispensable for development of the lymphatic system. *Mol Cell Biol*. 2005;25(6):2441–2449.
35. Alitalo AK, et al. VEGF-C and VEGF-D blockade inhibits inflammatory skin carcinogenesis. *Cancer Res*. 2013;73(14):4212–4221.
36. Karkkainen MJ, et al. A model for gene therapy of human hereditary lymphedema. *Proc Natl Acad Sci U S A*. 2001;98(22):12677–12682.
37. Tammela T, et al. Blocking VEGFR-3 suppresses angiogenic sprouting and vascular network formation. *Nature*. 2008;454(7204):656–660.
38. Haiko P, et al. Deletion of vascular endothelial growth factor C (VEGF-C) and VEGF-D is not equivalent to VEGF receptor 3 deletion in mouse embryos. *Mol Cell Biol*. 2008;28(15):4843–4850.
39. Haigh JJ, et al. Cortical and retinal defects caused by dosage-dependent reductions in VEGF-A paracrine signaling. *Dev Biol*. 2003;262(2):225–241.
40. Hayreh SS. Neovascular glaucoma. *Prog Retin Eye Res*. 2007;26(5):470–485.
41. Jeltsch M, et al. CCBE1 enhances lymphangiogenesis via ADAMTS3-mediated VEGF-C activation. *Circulation*. 2014;129(19):1962–1971.
42. Aihara M, Lindsey JD, Weinreb RN. Aqueous humor dynamics in mice. *Invest Ophthalmol Vis Sci*. 2003;44(12):5168–5173.
43. Petrova TV, et al. Transcription factor PROX1 induces colon cancer progression by promoting the transition from benign to highly dysplastic phenotype. *Cancer Cell*. 2008;13(5):407–419.
44. Wick N, et al. Transcriptomal comparison of human dermal lymphatic endothelial cells ex vivo and in vitro. *Physiol Genomics*. 2007;28(2):179–192.
45. Furumoto TA, et al. Notochord-dependent expression of MFH1 and PAX1 cooperates to maintain the proliferation of sclerotome cells during the vertebral column development. *Dev Biol*. 1999;210(1):15–29.
46. Muzumdar MD, Tasic B, Miyamichi K, Li L, Luo L. A global double-fluorescent Cre reporter mouse. *Genesis*. 2007;45(9):593–605.
47. Tammela T, et al. Angiopoietin-1 promotes lymphatic sprouting and hyperplasia. *Blood*. 2005;105(12):4642–4648.
48. Anisimov A, et al. Activated forms of VEGF-C and VEGF-D provide improved vascular function in skeletal muscle. *Circ Res*. 2009;104(11):1302–1312.
49. Enholm B, et al. Adenoviral expression of vascular endothelial growth factor-C induces lymphangiogenesis in the skin. *Circ Res*. 2001;88(6):623–629.
50. Saeki T, Aihara M, Ohashi M, Araie M. The efficacy of TonoLab in detecting physiological and pharmacological changes of mouse intraocular pressure — comparison with TonoPen and microneedle manometery. *Curr Eye Res*. 2008;33(3):247–252.
51. Zhou LX, Liu JHK. Circadian variation of mouse aqueous humor protein. *Mol Vis*. 2006;12:639–643.